

Mechanisms and Machine Science

Tongtong Liu · Fan Zhang ·
Shiqing Huang · Jingjing Wang ·
Fengshou Gu *Editors*

Proceedings of the TEPEN International Workshop on Fault Diagnostic and Prognostic

TEPEN2024-IWFDP - Volume 3



 Springer

Series Editor

Marco Ceccarelli, *Department of Industrial Engineering, University of Rome Tor Vergata, Roma, Italy*


Advisory Editors

Burkhard Corves, *RWTH Aachen University, Aachen, Germany*

Victor Glazunov, *Mechanical Engineering Research Institute, Moscow, Russia*

Alfonso Hernández, *University of the Basque Country, Bilbao, Spain*

Tian Huang, *Tianjin University, Tianjin, China*

Juan Carlos Jauregui Correa , *Universidad Autonoma de Queretaro, Queretaro, Mexico*

Yukio Takeda, *Tokyo Institute of Technology, Tokyo, Japan*

Sunil K. Agrawal, *Department of Mechanical Engineering, Columbia University, New York, USA*

This book series establishes a well-defined forum for monographs, edited Books, and proceedings on mechanical engineering with particular emphasis on MMS (Mechanism and Machine Science). The final goal is the publication of research that shows the development of mechanical engineering and particularly MMS in all technical aspects, even in very recent assessments. Published works share an approach by which technical details and formulation are discussed, and discuss modern formalisms with the aim to circulate research and technical achievements for use in professional, research, academic, and teaching activities.

This technical approach is an essential characteristic of the series. By discussing technical details and formulations in terms of modern formalisms, the possibility is created not only to show technical developments but also to explain achievements for technical teaching and research activity today and for the future.

The book series is intended to collect technical views on developments of the broad field of MMS in a unique frame that can be seen in its totality as an Encyclopaedia of MMS but with the additional purpose of archiving and teaching MMS achievements. Therefore, the book series will be of use not only for researchers and teachers in Mechanical Engineering but also for professionals and students for their formation and future work.

The series is promoted under the auspices of International Federation for the Promotion of Mechanism and Machine Science (IFTToMM).

Prospective authors and editors can contact Mr. Pierpaolo Riva (publishing editor, Springer) at: pierpaolo.riva@springer.com

Indexed by SCOPUS and Google Scholar.

Tongtong Liu · Fan Zhang · Shiqing Huang ·
Jingjing Wang · Fengshou Gu
Editors

Proceedings of the TEPEN International Workshop on Fault Diagnostic and Prognostic

TEPEN2024-IWFDP - Volume 3

Editors

Tongtong Liu
School of Mechanical Engineering
Inner Mongolia University of Science
and Technology
Baotou, China

Shiqing Huang
School of Industrial Automation
Beijing Institute of Technology
Zhuhai, China

Fengshou Gu
Department of Engineering and Technology
University of Huddersfield
Huddersfield, UK

Fan Zhang
School of Design
Southwest Jiaotong University
Chengdu, China

Jingjing Wang
School of Management Engineering
Qingdao University of Technology
Qingdao, China

ISSN 2211-0984

ISSN 2211-0992 (electronic)

Mechanisms and Machine Science

ISBN 978-3-031-69482-0

ISBN 978-3-031-69483-7 (eBook)

<https://doi.org/10.1007/978-3-031-69483-7>

© The Editor(s) (if applicable) and The Author(s), under exclusive license
to Springer Nature Switzerland AG 2024

This work is subject to copyright. All rights are solely and exclusively licensed by the Publisher, whether the whole or part of the material is concerned, specifically the rights of translation, reprinting, reuse of illustrations, recitation, broadcasting, reproduction on microfilms or in any other physical way, and transmission or information storage and retrieval, electronic adaptation, computer software, or by similar or dissimilar methodology now known or hereafter developed.

The use of general descriptive names, registered names, trademarks, service marks, etc. in this publication does not imply, even in the absence of a specific statement, that such names are exempt from the relevant protective laws and regulations and therefore free for general use.

The publisher, the authors and the editors are safe to assume that the advice and information in this book are believed to be true and accurate at the date of publication. Neither the publisher nor the authors or the editors give a warranty, expressed or implied, with respect to the material contained herein or for any errors or omissions that may have been made. The publisher remains neutral with regard to jurisdictional claims in published maps and institutional affiliations.

Responsible Editor: Pierpaolo Riva

This Springer imprint is published by the registered company Springer Nature Switzerland AG
The registered company address is: Gewerbestrasse 11, 6330 Cham, Switzerland

If disposing of this product, please recycle the paper.

Contents

Welding Quality Target Detection Based on YOLOv9 Lightweight Model	1
<i>Mingzhu Fu, Hongjun Wang, Wenxian Yang, Fan Jiang, Zeyu Ma, and Yanyan Cui</i>	
An Improved Residual Network for Bearing Fault Diagnosis in Strong Noise Background	13
<i>Zhilei Zhao, Jie Tao, Dalian Yang, Heyuan Jiang, Zihui Cao, and Piao Yang</i>	
Residual Life Prediction of Rolling Bearings Based on Transformer-BiGRU-Attention Model with Improved Sparrow Optimization Algorithm	23
<i>Xunmeng An, Chao Zhang, Caiye Liu, Guiyi Liu, and Jinzhang Hao</i>	
Effects of Cage Flexibility and Crack Propagation on Roller-Cage Pocket Interaction Forces and Dynamics in Cylindrical Roller Bearings	34
<i>Zhifeng Shi, Lan Luo, Gang Zhang, Changfeng Yan, and Jing Liu</i>	
A Review of Short-Term Wind Power Forecasting Based on Artificial Intelligence Methods	48
<i>Yangtian Zhang, Yunfei Ding, Youren Zhang, and Fudi Ge</i>	
Digital Twin System Based on NoSQL Database	60
<i>Feiyang Weng, Hongjun Wang, Fan Jiang, Mingzhu Fu, Yanyan Cui, and Zeyu Ma</i>	
Transmission Line Detection Method Based on Improved Res2Net-YOLACT Model	71
<i>Qiancheng Sun, Yunfei Ding, Qifan Chen, and Kun Tian</i>	
Variational Mode Decomposition Guided by Time-Frequency Domain Difference Information	81
<i>Hongbo Fei, Chao Zhang, Shuai Xu, Jing Zhang, and Le Wu</i>	
Tool Wear Prediction Based on Ball-End Milling Tool Milling Area	95
<i>Jiacheng Liu, Hongjun Wang, Wenxian Yang, Zheng Wang, Yanyan Cui, and Mingzhu Fu</i>	

Friction Torque of Four-Point Contact Ball Bearings Based on Dynamic Model	107
<i>Hui Xi, Tao Lin, Tian Ran Lin, Yu Jiang, and Yajun Shang</i>	
Dynamic Modeling and Analysis of a Planetary Gear System with a Tooth Chip Fault	116
<i>Jingping Sui, Yi Yang, Niaoqing Hu, and Zhe Cheng</i>	
Electromagnetic Design and Analysis of DC Solenoid Valve	128
<i>Shuai Xu, Yinhang Ning, Benqing Lv, and Zhihao Huang</i>	
A Fault Early Warning Method for Coal Mills Based on Causality and LSTM Model	140
<i>Chenlong Feng, Xin Zou, Chao Liu, and Dongxiang Jiang</i>	
A Review of Spiking Neural Network Research in the Field of Bearing Fault Diagnosis	151
<i>Yusen Wang, Hongjun Wang, Long Xie, Henglin Ge, Mingyang Zhou, Tao Chen, and Yuxing Shi</i>	
Dynamic Compensation Method for CNC Crankshaft Grinding Machine	166
<i>Peishuo Zhang, Hongjun Wang, and Henglin Ge</i>	
Multi-channel Parallel Computing in Capsule Network and Its Application in Mechanical Fault Diagnosis	180
<i>Haiwen Qiu, Jie Tao, Zhao Xiao, and Wenxian Yang</i>	
Feature Density Model-Based Abnormal Vibration Detection and Severity Assessment for Rotating Equipment	190
<i>Yaqiang Jin, Peng Chen, Meng Rao, Tian Ran Lin, and Ming J. Zuo</i>	
Initial Phase Determination Method for Vibration Separation Technology of Planetary Gear Train	201
<i>Yitao Jin, Zhi Wang, Fujian Xu, Hongtai Zhang, and Yun Liao</i>	
Research on Rolling Bearing Fault Diagnosis Method of Fuzzy Broad Learning System Based on Genetic Algorithm Optimization	208
<i>Le Wu, Chao Zhang, Hongbo Fei, Feifan Qin, Guiyi Liu, Shuai Xu, Bing Ouyang, Yangbiao Wu, and Jing Zhang</i>	
Research on Remaining Useful Life Prediction Method of Rotating Machinery Based on the Fusion of GRU and Transformer	219
<i>Zehua Fan, Changbo He, Yali Zhi, Yawei Hu, and Yongbin Liu</i>	

Multivariate Empirical Wavelet Transform and Its Application to Rolling Bearings	229
<i>Zhi Wang, Yitao Jin, Songtao Zhang, Shijun Cao, and Yun Liao</i>	
A Digital Twin Method for Marine Engines Based on PSO Algorithm	236
<i>Xiaomin Zhang, Shuying Li, and Yunpeng Cao</i>	
Study on Rolling Bearing Wear Experiment with Multi-source Information Monitoring	246
<i>Yi Pan, Yunpeng Cao, and Shuying Li</i>	
An Order Demodulation Analysis Method for Planetary Gearboxes	255
<i>Jiwei Chen, Ruitong Xie, Songsong Zhu, Mengxiong Zhao, Zhiyuan Wang, and Mian Zhang</i>	
Research on Identification Strategy of Fault-Sensitive Frequency for Planetary Gearboxes	267
<i>Ruitong Xie, Mian Zhang, Jiwei Chen, Songsong Zhu, Zhiyuan Wang, Mengxiong Zhao, and Hongbiao Xiang</i>	
Self-adhesive Fibre Bragg Grating Strain-Free Temperature Sensor for Temperature Measurement in Vibration Environment	279
<i>Chenxi Liu, Pingyu Zhu, Tingyu Huang, and Dejie Chen</i>	
Research on Few-Shot Sample Fault Prediction Method for Electric Drive Systems Based on Transfer Learning	285
<i>Shichen Zhang, Zizhen Qiu, Lingxiao Zhao, Xin Huang, Fang Wang, and Yang Kang</i>	
Research on Modulation Mechanism of Planetary Gear Set Considering Time-Varying Transmission Paths with Manufacturing Error	296
<i>Hongxiang Jing, Guojin Feng, Long Chen, Hao Zhang, Dong Zhen, and Fengshou Gu</i>	
Analysis of Battery Capacity Decay and Capacity Prediction	309
<i>Yan Gao, Xiaolei Shi, Fang Wang, Shiqiang Liu, Tianyi Ma, Pengfei Yan, and Ce Han</i>	
Intelligent Fault Diagnosis of Rolling Bearing Based on DGAC-SNN	325
<i>Shilong Zhu, Yiqing Yang, Ronghai Wei, Weiguo Huang, and Jun Wang</i>	
A Novel Contrastive Pre-training-Based Domain Adaptation Method for Fault Diagnosis of Rotating Machines	338
<i>Jungang Cao, Qing Zhang, Weiliang Cai, Zhe Yang, Yunwei Huang, Jianyu Long, Ping Wang, and Chuan Li</i>	

Gas Turbine Rotor Fault Diagnosis Based on Domain Adversarial Adaptation Transfer Learning for Small Samples	346
<i>Shucong Liu and Hongjun Wang</i>	
Accuracy of Instantaneous Angular Speed Signals for Fault Diagnosis of Planetary Gears: A Review	360
<i>Longda Yao, Xiaoli Tang, Lei Hu, and Yuandong Xu</i>	
Research on Battery State Estimation and Prediction Model Construction	369
<i>Yan Gao, Xiaolei Shi, Fang Wang, Shiqiang Liu, Tianyi Ma, Pengfei Yan, and Ce Han</i>	
An Approach for Infrasound Event Classification Based on DenseNet-BiLSTM Fusion and Self-attention Mechanism	385
<i>Zhicong Pang, Guojin Feng, Jirui Zhu, Jinzhen Kong, Dong Zhen, and Pengxiao Teng</i>	
An Investigation of Active Noise Control Based on Wave-U-Net	397
<i>Yamin Li, Guojin Feng, Guohua Sun, Dong Zhen, Hao Zhang, and Fengshou Gu</i>	
A Survey on Optimal Frequency Band Selection for Resonant Modulation Based Planetary Gear Fault Diagnosis	410
<i>Mu Wang, Yuandong Xu, Lei Hu, Guangfu Bin, Xiaoli Tang, and Anhua Chen</i>	
Loosening Bolt Detection of Sling Cars Based on Deep Learning and Feature Matching	420
<i>Kaifan Qiao, Guojin Feng, Dong Zhen, Xiaoxia Liang, Zhaozong Meng, and Fengshou Gu</i>	
A Review of Dynamic Analysis and Fault Diagnosis for Split-Torque Transmission System	429
<i>Weixin Yang, Zhi Wang, Mei Yin, Lei Hu, and Yuandong Xu</i>	
RUL Prediction of Split Torque Transmission System Using Particle Filtering and Degenerate Model	441
<i>Weixin Yang, Zhi Wang, Xin Tang, Lei Hu, and Yuandong Xu</i>	
Health Assessment of Split Torque Transmission System Using Improved Generative Adversarial Networks	450
<i>Zhi Wang, Niaoqing Hu, Fujian Xu, Yi Yang, and Lei Hu</i>	

Lightweight-Based Defect Detection for Small Target Insulators	463
<i>Shuxin Liu, Lei Zhang, Chengcheng Shi, Shuhan Qin, Guanjun Ji, and Xiaodi Wang</i>	
A Two-Stage Intelligent Model for State of Health Estimation of EV Lithium-Ion Battery at Variable Temperatures	473
<i>Xiaoyu Zhao, Zuolu Wang, Haiyan Miao, Wenxian Yang, Fengshou Gu, and Andrew D. Ball</i>	
Dynamic Modeling and Analysis of Helicopter Transmission System Considering the Effect of Input Conditions	486
<i>Lin Yang, Jingping Sui, Xiaolan Hu, Fengqiang Qian, and Lei Hu</i>	
Dynamic Characterization and Fault Identification of Planetary Gear Systems Under Transient Loads	498
<i>Long Chen, Dong Zhen, Zhanbo Cui, Guojin Feng, Hao Zhang, and Fengshou Gu</i>	
A Lightweight Parallel Convolutional Model for Abnormal Detection and Classification of Universal Robots Under Varied Load Conditions	512
<i>Yang Guan, Zong Meng, Samuel Ayankoso, Fengshou Gu, and Andrew Ball</i>	
Lubrication State Monitoring of Journal Bearings Based on Vibration Features	522
<i>Mengdi Li, Peiming Shi, Dongying Han, Zhifeng Hu, Yang Chen, Fengshou Gu, and Andrew D. Ball</i>	
Lubrication Effects on Rolling Bearing Dynamics: Modelling and Analysis	532
<i>Zewen Zhou, Xue Gong, Kunzuo Zhong, Bingyan Chen, Guojin Feng, Zhifeng Hu, Fengshou Gu, and Andrew Ball</i>	
Laser Spot-Assisted Long-Distance Visual Measurement of Structural Vibration	543
<i>Guanhua Yi, Rongfeng Deng, Yanling Cao, Baoshan Huang, and Fengshou Gu</i>	
Research on Buck Converter Based on Double Close-Loop ADRC	551
<i>Wenyong Wu, Sanbo Pan, and Xin Qiao</i>	
Experimental Investigation on Condition Monitoring of Journal Bearing Lubrication Status Based on On-Rotor Sensing Signal	561
<i>Zhifeng Hu, Mengdi Li, Yang Chen, Solomon Okhionkpanwonyi, Hao Zhang, Zewen Zhou, Fengshou Gu, and Andrew D. Ball</i>	

Digital Twin System for Condition Monitoring and Control of Unmanned Autonomous Vehicle Powertrain 571
Haibo Hong, Xin Chen, Shisong Wei, Guoji Shen, and Xinhao Shu

Research on the Turn Life Testing System for the Nose Landing Gear of Carrier-Based Aircraft 579
Bo Xu, Chaoze Zhao, Bo Gong, Chunyu An, and Xiaodong Wen

Author Index 595



Welding Quality Target Detection Based on YOLOv9 Lightweight Model

Mingzhu Fu^{1,2}, Hongjun Wang^{2,3}✉, Wenxian Yang⁴, Fan Jiang^{2,3}, Zeyu Ma^{1,2}, and Yanyan Cui^{1,2}

¹ School of Mechanical Engineering, Beijing University of Information Science and Technology, Beijing 102206, China

605602794@qq.com

² Beijing International Science Cooperation Base of High-End Equipment Intelligent Perception and Control, Beijing 100192, China

wanghongjun@bistu.edu.cn

³ School of Information Management, Beijing University of Information Science and Technology, Beijing 102206, China

⁴ Centre for Efficiency and Performance Engineering, University of Huddersfield, Hudders-Field HD1 3DH, UK

Abstract. To tackle the challenges of low accuracy, inefficiency, and data processing complexities inherent in traditional welding quality detection methods, we employ the Yolov9 lightweight model to precisely identify and detect key defects, such as cracks and holes. We perform detailed annotation work on the dataset to ensure data quality, and during detection, utilize Anchor boxes and a range of data augmentation techniques to improve the accuracy and robustness of the model. Through strict training and analysis of the data set, the parameters and structure of the model are constantly adjusted, after a large number of tests and verification, the average accuracy of the model training results can reach 98.7%, and the evaluation indicators such as Accuracy, Recall and main Average Precision also perform well, and the optimized model has the characteristics of fast, accurate and lightweight. The experimental results show that the model shows high accuracy and stability in detecting welding defects, and can effectively identify various defect types in the weld, and accurately determine their position and size. This result not only proves the effectiveness of the Yolov9 model in welding nondestructive testing, but also provides a reliable basis for the subsequent practical application.

Keywords: Deep Learning · YOLOv9 · Object Detection · Welding Defect

1 Introduction

In recent years, deep learning has made remarkable achievements in the fields of image recognition, speech recognition, natural language processing and so on, fully demonstrating its great application value and potential [1]. Especially in the field of target detection, deep learning model has become the core of research and application. As one of the key research directions of computer vision, target detection algorithm based

on deep learning dominates for its efficient and accurate detection performance [2]. By learning and analyzing the feature expression in a large amount of data, the deep learning model can automatically extract and abstract the key features from the image, so as to realize the accurate identification and positioning of the target [3]. Given the unique advantages of the target detection technology, this study decided to apply it to the field of welding defect detection.

With the continuous development of industrial technology, welding, as an important means to connect the metal structure, the accuracy and efficiency of its quality detection is of great significance for ensuring the product quality and production safety. Traditional welding quality testing methods have problems such as low accuracy, low efficiency and difficult data processing, which is difficult to meet the demand of modern industrial production [4]. In contrast, the welding quality detection method based on deep learning model has better adaptability and robustness, and can effectively cope with the challenges such as diverse welding shapes and complex light conditions. At present, many studies have tried to use deep learning model for welding quality detection. Say et al. proposed an automatic method to identify multiple types of welding defects by processing X-ray images, which is realized through intelligent fusion of data enhancement technology and convolutional neural network [5]. Guo et al. proposed a welding defect classification method based on lightweight convolutional neural network, which reduces structural parameters under the premise of ensuring classification accuracy, and visualizes the feature data of each convolutional layer, which improves the interpretability of the model [6]. Lei et al. used experimental data and simulated data to train Bayesian regularization neural network (BRNN) and CNN to predict weld quality classification in ultrasonic welding, and showed that BRNN and CNN have similar classification accuracy, but compared with BRNN, CNN has advantages in training efficiency. These studies use convolutional neural network to identify and classify weld defects, and have achieved good results [7].

In the classic target detection YOLO series model [8], the researchers are committed to optimizing the network structure to improve the detection of small target defect signal, including Xu et al. Study small defects in pipe surrounding weld detection, using convolution block attention module (CBAM) to optimize the YOLOv5 network model structure, so as to improve the detection network is to extract small target defect signal preference [9]. However, Shen et al. optimized the model by improving the C3 module in YOLOv5 [10], while Zhen et al. adopted the ELAN structure based on gradient path design, combined with deep separable convolution and Ghostv2 module to lightweight the YOLOv5 model [11]. In the application of YOLOv7, Li et al. proposed to improve the YOLOv7-tiny shaft sleeve surface defect detection algorithm to improve the detection accuracy and efficiency of the shaft sleeve surface defects [12]. Xu et al. proposed an improved YOLOv7 model to reduce the leakage rate of pipe weld surface defects [13]. In the application of YOLOv8, Su et al. proposed an improvement of YOLOv8 intelligent detection method to improve the efficiency and accuracy of automatic detection of digital ray imaging of aviation aluminum alloy welding defects [14]. However, these methods usually require a large number of annotation data training, and model complexity and computation is larger, based on this, this study using YoloV9 lightweight model jointly developed by Taiwan, China Academia sinica and Taipei university of

science and technology for welding quality detection [15], YOLOv9 model proposed programmable gradient information (PGI) and general high efficiency layer aggregation network (GELAN) architecture. PGI ensures that the model maintains the key features of deep features during training, avoiding the problem of semantic loss, while GELAN achieves higher parameter usage through traditional convolution, making the model more lightweight, fast and accurate. In this study, YOLOv9 model is used for welding defect detection, which aims to ensure the accuracy of defect detection, thus improving the detection efficiency.

2 Experimental Principle

2.1 YOLOv9 Design Principle

YOLOv9 As a new generation of real-time target detection system, its design principle is simple and powerful. The algorithm transforms the target detection task into a single forward propagation process, which enables the whole target detection process to be completed in a forward propagation, and has obvious advantages in speed over the traditional target detection algorithm. Secondly, the input image is usually a convolutional neural network, which is transformed into a feature graph and performs target detection on the feature graph at different scales. Key design features include the use of Anchor boxes to assist target positioning, Anchor boxes is a pre-defined set of bounding boxes that capture targets of different sizes and proportions, and YOLOv9 simultaneously predicts the offset and size of these boxes when predicting target frames, thus enabling more accurate target positioning. In addition, YOLOv9 adopts a series of data enhancement techniques and training strategies to improve the robustness and generalization ability of the model, such as random scaling, cropping, color transformation, etc. Through the combination of these design principles, YOLOv9 can achieve accurate and fast target detection while maintaining high efficiency, becoming one of the important algorithms in the field of target detection. The formulas involved in the core module are as follows:

- 1) Convolution operations: Convolution operations are used to extract features from the input feature graph.

$$Y = W * X + b \quad (1)$$

where X is the input feature graph, W is the convolution kernel, b is the offset top, and $*$ is the output feature graph, representing the convolution operation.

- 2) Batch normalization: Batch normalization is used to speed up the training process and improve the generalization ability of the model.

$$\hat{x}_i = \frac{x_i - \mu}{\sqrt{\sigma^2 + \epsilon}} \quad (2)$$

$$y_i = \gamma \hat{x}_i + \beta \quad (3)$$

where x_i represents the i th element in the input data, μ is the mean of the input data, σ is the standard deviation of the input data, γ and β are learnable scaling and offset parameters, and ϵ is a small constant for numerical stability.

- 3) Activation function: The activation function is used to introduce nonlinear characteristics to increase the expression power of the model.

$$f(x) = \max(0, x) \quad (4)$$

The ReLU (Rectified Linear Unit) function sets the negative input value to zero and keeps the positive value constant.

$$f(x) = \frac{1}{1 + e^{-x}} \quad (5)$$

The Sigmoid function is an S-shaped function that maps the real number to the (0,1) interval.

$$f(x) = \frac{e^x - e^{-x}}{e^x + e^{-x}} \quad (6)$$

The Tanh function is also an S-shaped function, similar to the Sigmoid function, but its output range is (-1,1).

- 4) Target detection loss function: The commonly used loss functions in target detection tasks include classification loss, localization loss, and confidence loss. Their mathematical expressions are as follows:

$$L_{cls} = -\frac{1}{N_{obj}} \sum_{i=0}^{S^2} \sum_{j=0}^B 1_{ij}^{obj} \log(\hat{p}_i^c) \quad (7)$$

where N_{obj} is the number of targets in each image, S is the size of each feature graph, B is the number of bounding boxes in each cell, 1_{ij}^{obj} is an indicator variable indicating whether the i th cell contains targets, and \hat{p}_i^c is the predicted probability of the model for the target category.

$$L_{loc} = \frac{\lambda_{loc}}{N_{obj}} \sum_{i=0}^{S^2} \sum_{j=0}^B 1_{ij}^{obj} \left[\sum_{k \in \{x,y,w,h\}} \text{smooth}_{ij}^{loc}(k) \right] \quad (8)$$

where λ_{loc} is the weight of the localization loss, and $\text{smooth}_{ij}^{loc}(k)$ is the smooth $L1$ loss function used to calculate the loss of the bounding box coordinate k .

$$L_{conf} = -\frac{1}{N_{obj}} \sum_{i=0}^{S^2} \sum_{j=0}^B 1_{ij}^{obj} \log(\hat{p}_i^{obj}) + \lambda_{noobj} \sum_{i=0}^{S^2} \sum_{j=0}^B 1_{ij}^{noobj} \log(1 - \hat{p}_i^{obj}) \quad (9)$$

where \hat{p}_i^{obj} is the confidence of the model about the existence of the target, and λ_{noobj} is the weight of the loss of the target.

2.2 Model Architecture

YOLOv9 The model architecture diagram is shown in Fig. 1, drawn according to YOLOv9.yaml, and the detailed structure diagram of each module is shown in Fig. 2 [16].

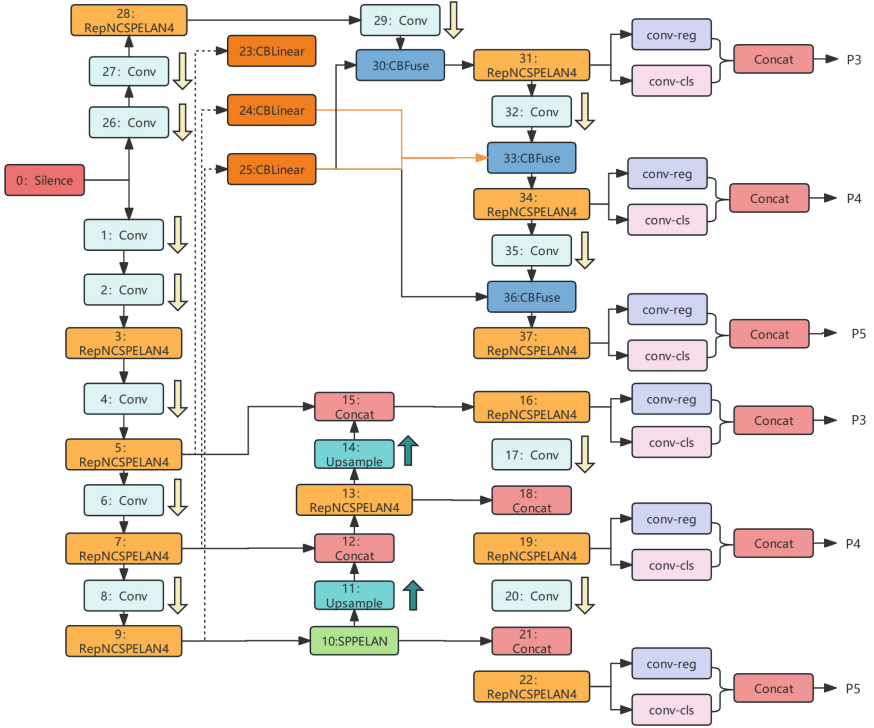


Fig. 1. Model architecture diagram.

Figure 1 shows the overall architecture of YOLOv9, which includes three major parts: feature extraction network, neck network and head network. The feature extraction network is responsible for extracting the features from the input images, and it is usually implemented by using the deep convolutional neural network (DCNN). The neck network is responsible for the further fusion and enhancement of the features extracted by the feature extraction network to improve the robustness and accuracy of the feature expression. The head network is responsible for target detection according to the fused features, including tasks such as target classification, positioning and confidence prediction.

Figure 2 illustrates the specific structure of the individual modules in the YOLOv9. Specifically, the feature extraction network CSPDarknet53 consists of multiple residual modules, each containing multiple convolution layer, batch normalization layer and activation function, to extract the features of the input image. The neck network contains multiple SPP modules and PANet structures, which are used to fuse and enhance the features extracted by the feature extraction network. The head network consists of multiple convolution layers, full connection layers and activation functions, which are used to achieve target classification, positioning and confidence prediction tasks.

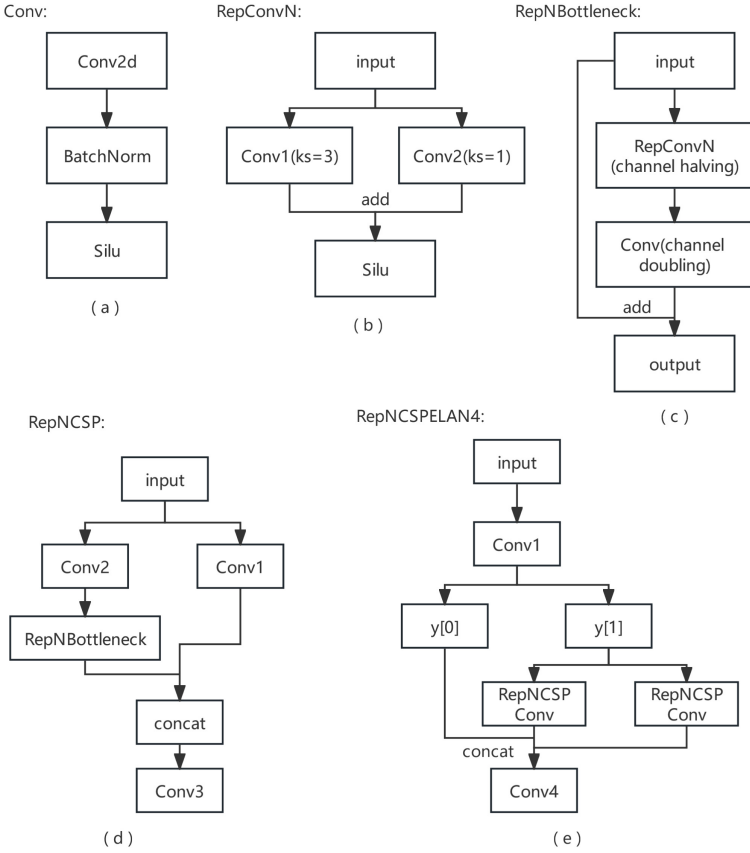


Fig. 2. Module structure diagram.

3 Experiment Procedure and Results

3.1 Experimentation

Selection of the Dataset. The data was collected by engineers engaged in the welding industry, ensuring the authenticity and representativeness of the data. The dataset covers three core welding surface types, including cracks, holes and normal types, reflecting the common defects in the welding process. To ensure the quality and versatility of the dataset, we performed an exhaustive screening and precise annotation work. In addition, a variety of expansion processing technologies, including data rotation, blur processing, brightness adjustment and protection adjustment, are adopted to simulate various situations that may occur in the actual scene. After careful arrangement and analysis, we finally obtained a set of high quality and universal welding surface data set, containing a total of 6854 pictures, including 1126 cracks, 5626 holes and 66 normal pictures. Figure 3 is a representative case of the defects and the normal conditions.

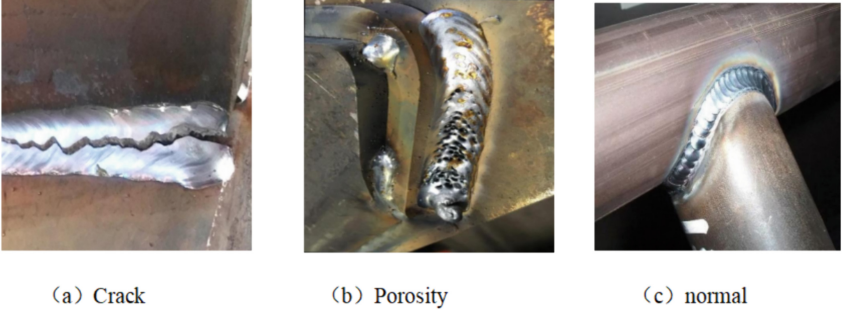


Fig. 3. Dataset types represent.

Training Process Setting. During the experiment, the YOLOv9 model was used to make full use of the aforementioned programmable gradient information (PGI) and general efficient layer aggregation network (GELAN) architecture. Following the standard training process, the data set was divided into the training set, validation set and test set. The training set was used to train the model, the validation set was used to adjust the hyperparameters and monitor the model performance, while the test set was used to evaluate the model performance on unseen data. Secondly, we pre-processed the dataset, including the steps of normalization and data enhancement, to improve the generalization ability of the model. During the training process, the stochastic gradient descent (SGD) optimizer is used to train the model, and the appropriate hyperparameters such as learning rate and momentum are set. To prevent overfitting, we used an early-stop strategy at the end of training, which terminated training early when the validation set performance no longer improved. This strategy helps to improve the generalization performance of the model and ensure that it performs well on unknown data.

3.2 Model Evaluation

It is very important to evaluate the model after the training. Evaluation the model can help verify the generalization ability of the model, guide the further optimization of the model training strategy, hyperparameter adjustment and network architecture design, and improve the performance and robustness of the model. The mathematical expressions for the common evaluation indexes are shown below:

- 1) mAP: Average accuracy is a commonly used evaluation index in the target detection task, which comprehensively takes into account the precision and recall rate of the detection results. The process of calculating the average accuracy includes calculating the AP (Average Precision) for each category at different confidence thresholds, and then taking the AP across all categories.

$$mAP = \frac{1}{N} \sum_{i=1}^N AP_i \quad (10)$$

where N is the number of categories, AP_i is the average accuracy of category i .

- 2) Recall: recall refers to the ratio of the number of positive samples detected by the model to the total number of positive samples. In the target detection task, the proportion of targets detected by the model to all true targets.

$$Recall = \frac{TP}{TP + FN} \quad (11)$$

where TP is the true example (number of targets correctly detected by the model) and FP is the false negative example (number of targets that the model failed to detect).

3.3 Experimental Results

Table 1 shows the performance indicators of the model in various categories, including accuracy (P), recall (R), mAP 50, and mAP 5095. These indicators collectively reflect the performance of the model in detecting different types of welding surface defects. As can be seen from the table, the model has the best performance in the Crack category, with P and R close to 1, and mAP 50 and mAP 5095 are relatively high, reaching 0.987 and 0.834 respectively, showing the high sensitivity of the model to this type of welding surface defects. This may be because the crack defects are more obvious in the image, and the model can identify and locate more accurately. In the Porosity category, the performance of the model decreased slightly, but still maintained high P and R, and mAP 50 and mAP 5095 also performed well. For the Normal category, the model performance was relatively low, with P and R slightly lower than the other categories.

Table 1. Model performance indicators.

Class	Images	Instances	P	R	mAP50	mAP 5095
All	372	1414	0.851	0.824	0.825	0.586
Crack	372	236	0.983	0.972	0.987	0.834
Porosity	372	1165	0.823	0.815	0.842	0.563
Normal	372	13	0.748	0.686	0.648	0.359

In Fig. 4, we display performance curves for the model on the welded surface dataset, including Precision-Recall and mAP-Recall. These curves visually illustrate the model's performance at various thresholds. Notably, the Precision-Recall curve indicates the model's strong performance in detecting crack and hole categories, with high recall and accuracy, verified by its position near the upper right corner. Additionally, the mAP-Recall curve demonstrates the model's ability to maintain high average accuracy, particularly evident in crack detection, showcasing its sensitivity to this defect type.

In Fig. 5, the ROC and PR curves provide a comprehensive assessment of the model's performance at varying thresholds. The ROC curve evaluates classification performance, with the model's curve positioned close to the upper left corner for crack and hole detection, indicating high True Positive Rate and low False Positive Rate, thus accurately distinguishing defects. Similarly, the PR curve, depicting Precision against Recall,

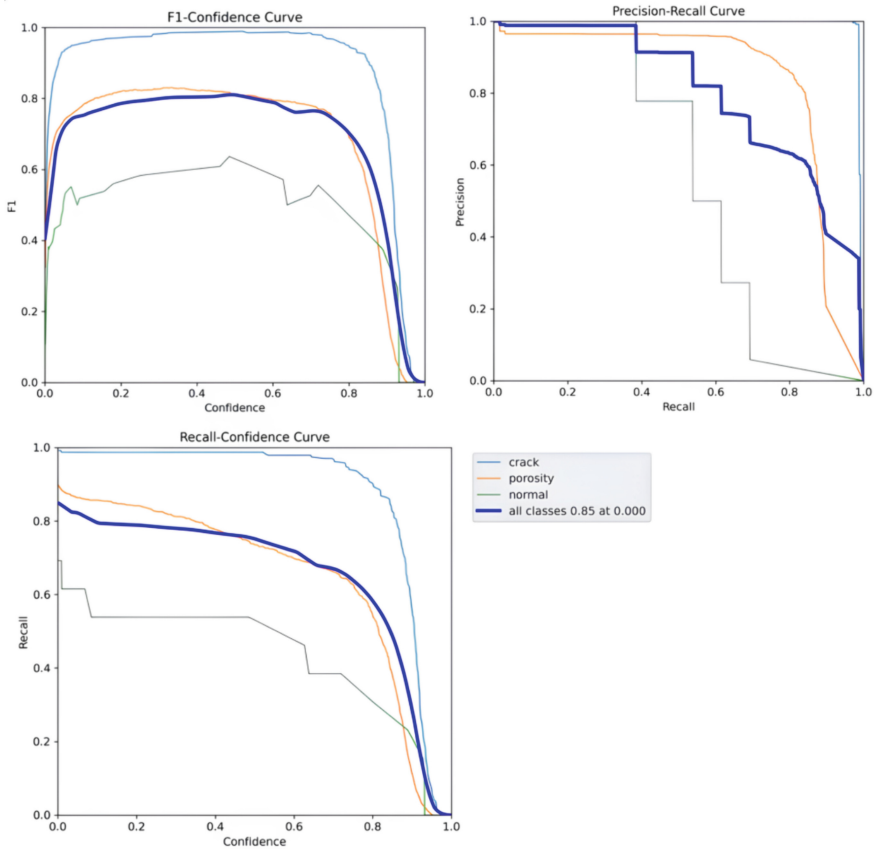


Fig. 4. Model performance curve.

showcases the model's high recall and precision, particularly evident in crack and hole detection, further validating its performance in identifying these defects.

In Fig. 6, we present index curves for the model's performance on the welding surface dataset, encompassing Accuracy, Recall, F1 Score, and AUC-ROC. These curves offer a comprehensive evaluation of the model's performance across varying training iterations or thresholds. With increasing iterations, the model's accuracy steadily improves and stabilizes, indicating effective feature learning. Similarly, the recall curve illustrates the model's increasing ability to detect defect regions, achieving high recall. The F1 score, a harmonic mean of accuracy and recall, demonstrates balanced performance, gradually improving and stabilizing with iterations. The AUC-ROC curve shows the model's overall performance across thresholds, steadily increasing and stabilizing, indicating consistent performance across various thresholds.

In Fig. 7, we showcase the YOLOv9 model's actual detection performance in weld quality assessment. These images vividly illustrate the model's capability to detect and locate weld defects, even in small or irregular shapes, thanks to the powerful feature

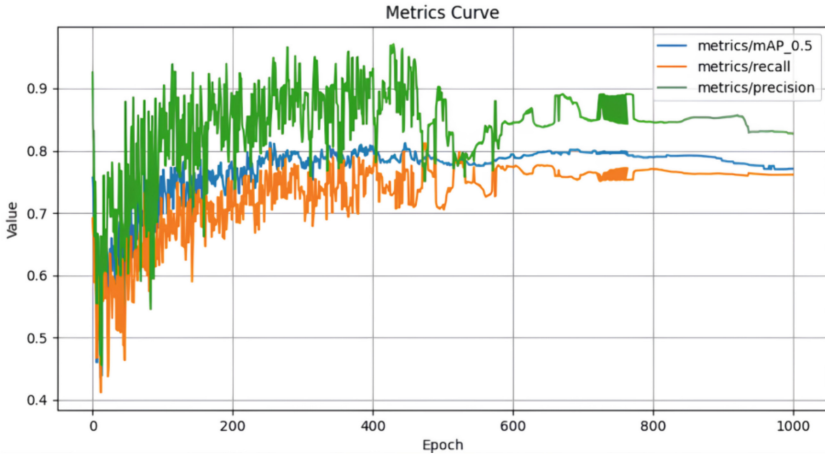


Fig. 5. Model performance evaluation curve.

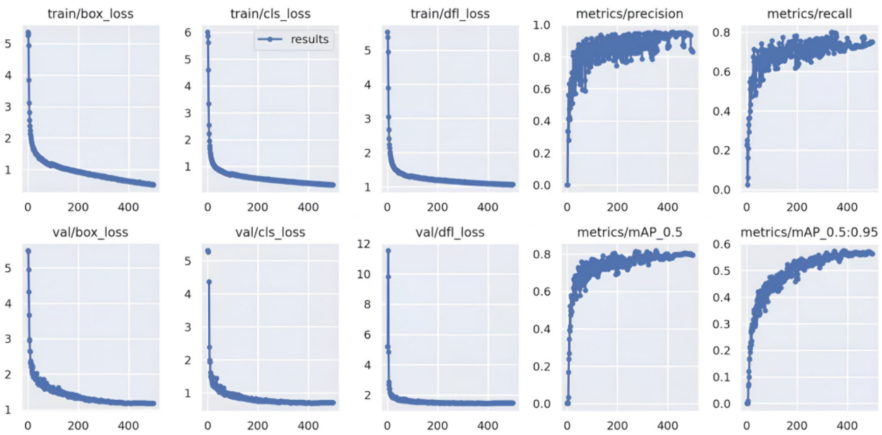


Fig. 6. Indicator curve.

extraction and accurate boundary box regression of the YOLOv9 algorithm. Additionally, despite complex industrial environments such as oil pollution and rust, the model accurately identifies defects and filters out background interference, showcasing its adaptability and robustness trained across diverse scenarios.



Fig. 7. Detection effect display

4 Conclusion

This study employs the YOLOv9 algorithm-based detection model to effectively identify and position weld defects, demonstrating high accuracy, recall, and F1 scores, particularly for crack and hole categories, with AUC-ROC values indicating stable performance across various thresholds. The optimized YOLOv9 model exhibits characteristics of speed, accuracy, and lightweight, making it adaptable to real-time detection needs in production environments. Despite its promising performance, challenges remain, such as the need to address missed detections for special defect types by enriching the dataset. Future research will focus on further optimizing the model structure and parameters, integrating with hardware accelerators to enhance reasoning speed, exploring cloud computing and big data technologies for remote monitoring and management of weld quality, and enhancing model interpretability to improve user trust.

Acknowledgement. This research is supported by Beijing Science and Technology Plan Project (Grant No. Z201100008320004) and the National Natural Science Foundation of China (Grant No. 51975058).

References

1. Manakitsa, N., Maraslidis, G.S., Moysis, L., Fragulis, G.F.: A review of machine learning and deep learning for object detection. Semantic Segmentation, and Human Action Recognition in Machine and Robotic Vision. Technologies (2) (2024)
2. Cai, J., Mao, Z., Li, J., Wu, X.: Overview of object detection algorithms and applications based on deep learning. Network Security Technol. Appl. (11), 41-45 (2023)
3. Chen, K., Zhu, Z., Deng, X., Ma, C., Wang, H.: Summary of deep learning studies on multi-scale object detection. Software J. (04), 1201-1227 (2021)
4. Xu, D., Wang, L., Li, F.: Review of typical object detection algorithms for deep learning. Comp. Eng. Appl. (08), 10-25 (2021)

5. Say, D., Zidi, S., Qaisar, S.M., Krichen, M.: Automated categorization of multiclass welding defects using the x-ray image augmentation and convolutional neural network. *Sensors (Basel, Switzerland)* **23**(14), 6422 (2023)
6. Guo, B., Wang, Y., Li, X., Zhou, Y., Li, J., Rao, L.: Welding defect classification based on lightweight CNN. *Int. J. Pattern Recognition and Artificial Intelligence* **37**(11), 2350026 (2023)
7. Sun, L., Tan, C., Hu, S.J., Dong, P., Freiheit, T.: Quality detection and classification for ultrasonic welding of carbon fiber composites using time-series data and neural network methods. *J. Manufacturing Syst.* **61**, 562–575 (2021)
8. Ma, J., Huang, S., Jin, D., Wang, X., Li, L., Guo, Y.: LA-YOLO: an effective detection model for multi-UAV under low altitude background. *Measurement Science and Technol.* **35**(5), 055401 (2024)
9. Xu, L., et al.: Intelligent identification of girth welds defects in pipelines using neural networks with attention modules. *Eng. Appl. Artificial Intelligence (PB)* **127**, 107295 (2024)
10. Shen, W., Zhang, Z., Xu, K.: Detection of weld piece surface defects based on the improved YOLOv5. *Combined Machine Tools and Automatic Processing Technol.* (03), 124–128+132 (2024)
11. Zhen, G., Zhao, L., Li, W., Chuqun, Wang, D., Sun, Y.: Lightweight study of improving steel surface defect detection network of YOLOv5. *Combined Machine Tools and Automatic Processing Technol.* (03), 58-63 (2024)
12. Li, D., Sun, Y., Wang, P., Ye, M.: Improving YOLOv7-tiny. *Manufacturing Technology and Machine Tools* 1–11
13. Xu, X., Li, X.: Research on surface defect detection algorithm of pipeline weld based on YOLOv7. *Scientific Reports* (1), 1881–1881 (2024)
14. Su, Z., Huang, Z., Qiu, H., Guo, C., Yin, X., Wu, G.: Defect detection method of aviation aluminum alloy weld based on improved YOLOv8. *AerDynamics* 1–10
15. Wang, C.Y., Yeh, I.H., Liao, H.Y.M.: YOLOv9: Learning What You Want to Learn Using Programmable Gradient Information. arXiv preprint [arXiv:2402.13616](https://arxiv.org/abs/2402.13616), 2024 (2024)
16. LNCS Homepage. <https://blog.csdn.net/wuling129/article/details/136316576>. Accessed 27 Mar 2024



An Improved Residual Network for Bearing Fault Diagnosis in Strong Noise Background

Zhilei Zhao¹, Jie Tao¹(✉), Dalian Yang², Heyuan Jiang¹, Zhihui Cao¹, and Piao Yang¹

¹ School of Computer Science and Engineering, Hunan University of Science and Technology, Xiangtan 411201, China

yuruoxingchen@163.com, caroltao@hnust.edu.cn

² Hunan Provincial Key Laboratory of Health Maintenance for Mechanical Equipment, Hunan University of Science and Technology, Xiangtan 411201, China

Abstract. In bearing fault diagnosis, the residual network has achieved certain results. However, in strong noise environment, the fault diagnosis accuracy of traditional residual network is not high. Therefore, this article proposes an improved residual network with multi-channel (MCRN). In MCRN, each layer establishes a directly connection with input data, and forming a multi-channel feature extraction mode. Then, we design the multi-channel integration algorithm to extract fault features of signals. Thereby MCRN can obtain more complete fault information from input data. Experiments are conducted on the IMS datasets, and the effectiveness of MCRN is demonstrated. Compared with traditional methods, when the signal-to-noise ratio reaches -4 db, the accuracy of MCRN keeps over 95%.

Keywords: Residual Network · Multi-channel · Integration Aggregation · Bearing Fault Diagnosis

1 Introduction

Rolling bearings, as the key components in rotating machinery, are widely used in fields such as aerospace, electricity industry, metallurgy, and machinery. According to statistics, about 30% of mechanical failures are related to bearing damage [1]. If the bearing fault is not found timely, it will evolve into serious mechanical failure, even cause equipment damage, production stoppage and personnel casualties. Therefore, the bearing fault diagnosis has important theoretical and practical significance, which can ensure the safe operation of mechanical equipment [2, 3].

Residual neural network (ResNet) is one of the most important models in deep learning. It is proposed by four scholars from Microsoft Research, who won the competition in the ImageNet Large Scale Visual Recognition Challenge in 2015 [4]. ResNet can automatically extract useful information from massive data and pictures. So, ResNet has attracted increasing attention from academia and industrial communities [5]. They use residual networks to extract fault features from monitoring signals of mechanical equipment, and judge the operating status of bearings, and determine bearings' failures [6–8]. Hu et al. [9] advantaged prior knowledge to improve residual shrinkage prototype

network and solve the fault diagnosis challenge under limited labeled samples. He et al. [10] proposed an inverted residual convolutional network for flywheel bearing diagnosis, which was based on parameter optimization with variational mode decomposition. Zhang et al. [11] combined a threshold adaptive activation function into Residual Network for bearing fault diagnosis. Yan et al. [12] adopted multi-attention mechanism to improve residual network for mechanical fault diagnosis. Zhang et al. [13] used channel-spatial attention mechanism to improve the kernel election in deep residual network, which can fuse the signals' feature for mechanical fault diagnosis. Zhao et al. [14] constructed different structures of residual shrinkage networks and researched their affections for bearing fault diagnosis. Xu et al. [15] constructed spiking residual shrinkage network for bearing fault diagnosis and effectively improves the accuracy. Yu et al. [16] adopted ResNet-152 with multi-scale stacked receptive field in bearing fault reconstruction diagnosis and achieved good results. Wen et al. [17] used ResNet-50 to construct a transfer convolution neural network for fault diagnosis. From this, ResNet can mine the fault information in signals and directly establish a mapping between monitoring data and bearing status. Therefore, ResNet can achieve end-to-end fault diagnosis, eliminating the dependence of fault diagnosis methods on manual feature design and diagnostic experience.

However, in strong noise environments, the fault characteristics in signals are mixed with various noises, the various fault feature values of bearings are extremely similar. The bearing fault characteristics in the signal are inherently weak, and fault characteristics are easily masked by noise. To address this issue, we design multiple channels to improve the traditional residual networks (MCRN). In MCRN, it establishes direct connections between each hidden layer and input data, so it establishes a multi-channel learning mechanism in every hidden layer with the input signals. Each hidden layer utilizes multi-channel mechanism to reconstruct information from traditional process features and raw signals. So MCRN may more fully capture bearing fault features from original signals. Then experiments were conducted under different noise intensities, and the results showed that MCRN can more completely extract bearing fault information, thereby MCRN can improve the accuracy of bearing fault diagnosis in strong noise environments.

The structure of remaining parts can be depicted in the following structure. Section 2 introduced the theoretical basis of residual network. Section 3 provided the residual network with multiple channels. Section 4 elaborated the proposed fault diagnosis method. Section 5 showed the details of the experiments and results. Then a conclusion followed in the last section.

2 Theoretical Basis of Residual Network

ResNet, as a kind of deep convolutional neural network, it consists of multiple residual blocks in series. In ResNet, each convolutional layer does not directly map the input to the output, but through "shortcut connections", it spans several layers to add the input to the output. The core of residual neural networks is residual building blocks. The structure of the basic residual block is shown in Fig. 1, which is divided into two parts: direct mapping and residual part.

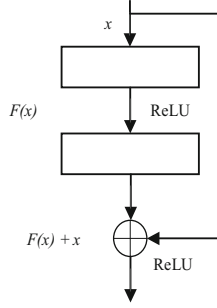


Fig. 1. Traditional Residual block structures.

The input of the residual block is x , the output is $H(x)$, the forward neural network layer is $F(x)$, and $F(x) = H(x) - x$. For example, when a forward neural network layer contains two weight layers, $F(x)$ and x are added element by element. As shown in the Eq. (1): $F(x, \{W_i\})$ is residual mapping to be learned; $F(\cdot)$ is residual function; W_1 and W_2 are weight parameters; σ is ReLU activation function.

$$\begin{cases} y = F(x, \{W_i\}) + x \\ F = W_2\sigma(W_1x) \end{cases} \quad (1)$$

When the two mappings' dimensions are different, firstly a linear mapping on x is performed to match the dimensions, then add them together. In the Eq. (2): W_s are the mapping weights of input x .

$$\begin{cases} y = F(x, \{W_i\}) + W_sx \\ F = W_2\sigma(W_1x) \end{cases} \quad (2)$$

When using the traditional residual block in bearing fault diagnosis, ResNet can establish the relationship between faults and vibration in a bottom-up feature extraction. And ResNet uses some activation functions and dropouts' techniques to improve the model's anti-interference ability. However, traditional residual block only adopts single kernel and additional operation to compute the feature value, when two-pixel values are added together, there is a situation of mutual cancellation, it may lead to useful information loss. Especially the simple bottom-up feature extraction, when the front layer fails to fully capture fault features, the back layer cannot contact the original signal and previous feature layers, which cannot compensate for the lost useful information, resulting in incomplete feature extraction and affect the accuracy of fault diagnosis.

3 Improved Residual Neural Network with Multi-channel

Due to the incomplete feature extraction of signals by traditional residual networks, we propose a multi-channel residual network model. The model consists of two parts: multi channels connection and channels integration. As shown in Fig. 2, the entire network consists of three channels, each channel contains multiple intermediate layers,

connection layers, and transition layers. Between various connection layers, we use integration operation for multi-channel cascading, and generate multiple transition layers during the integration process. The intermediate results of each transition layer are convolved and merged by the intermediate layer, and then the features are collected to the next connecting layer. The multi channels directly establishes links at various layers of the network, it allows input data to connect with each hidden layer, and the hidden layers are also interconnected. Then, we design an integration operation to control the computational complexity and parameter size, and it cascades each stacked feature with the original signals in each hidden layer.

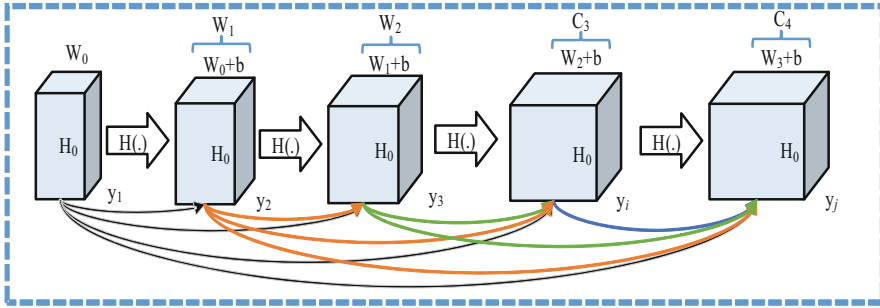


Fig. 2. Structure of multi-channel residual neural.

Firstly, the input layer is convolved with the convolution kernel to obtain a feature layer. The operation process is shown in Eq. (3).

$$y_j^l = \sum_i w_{i,j}^l \cdot x_i^{l-1} + b_j^l \quad (3)$$

Among them: y_j^l represents the output of the l -th layer, it concatenates the j -th layers and the i -th layer; $w_{i,j}^l$ represented as the weight of the convolutional kernel; x_i^{l-1} represented as the i th feature to be operated on in the $(l-1)$ -th layer; b_j^l is the bias value.

As a linear transformation, convolution operations cannot handle non-linear mapping relationships. In order to improve the non-linear processing ability of the model, the Leaky ReLU activation function is introduced to perform non-linear mapping on the convolutional output, enhancing the model's non-linear expression ability. Among them, the ReLU function sets values less than or equal to 0 to 0.1, which may cause gradient vanishing problems. The Leaky ReLU function optimizes the ReLU function by linearly interpolating the negative output, avoiding the problem of gradient vanishing that may cause the death of the convolution kernel. The ReLU function and Leaky ReLU function are shown in Eq. (4) and Eq. (5), respectively. Among them, a_j^l represents the activation value output by the convolutional layer of y_j^l . a is a lead parameter less than 1, usually taken as 0.01.

$$a_j^l = \max(0, y_j^l) \quad (4)$$

$$f(x) = \begin{cases} x, & x > 0 \\ ax, & x \leq 0 \end{cases} \quad (5)$$

Then each layer obtains additional inputs from all preceding layers, and passes on its own feature-maps to all subsequent layers. As shown in Eq. (3), the convolution layer l receives the feature-maps of all the layers, x_0x_{l-1} , as input:

$$x_l = H_{l,k}[Convolution(x_0, \dots, x_{l-1})] \quad (6)$$

where $H_{l,k}(\cdot)$ is the nonlinear transformation operation of layer l in MCRN. It can be a composite function such as BN, ReLU, and Conv. The term k refers to the number of feature maps, which produces by each function H_l . If each function H_l produces k feature-maps as output, it follows that the l -th layer has $k \times (l - 1) + k_0$ input feature-maps, where k_0 is the number of multi-channels. To prevent the network growing too wide, we limit k to a small integration and it can improve the parameters efficiency.

The multi-channel can make use of features from various angles, reduce the impact of noise on features, increase the output diversity. In addition, short-circuit connections are established between each layer to make the deep convolution and shallow convolution more closely connected. The output loss value can effectively constrain the optimization direction of parameters and accelerate the convergence speed of the network. Ultimately, multi-channel extracts the fault feature information more completely and comprehensive.

The overall flow chart is illustrated in Fig. 3. The yellow part is the data processing stage, which includes data acquisition, overlapping sampling, and STFT. The blue part is the fault diagnosis stage, which includes training of MCRN model and early diagnosis of bearing fault under strong noise environments.

Because MCRN is based on residual networks, it mainly extracts features and recognizes patterns from image information. As the two-dimensional spectrograms can simplify the complexity of the signal, making feature extraction easier. To this end, we use Fast Fourier Transform (FFT) to transform the original one-dimensional vibration signal into two-dimensional image data, which load into MCRN as the input data for bearing fault feature extraction and fault type recognition. Because the number of vibration signals collected in the experiments is limit, we use resampling to process the original vibration signals. The slide window size is 2048 and a slide step size is 100. Starting from the starting position, build a data sample using 2048 sampling points at a time by sliding the window.

After data preprocessing, the time-frequency graphs are input into the MCRN. The MCRN consists of an initial layer, four channels, three transition layers, and one classification layer. As shown in Table 1, the structure in multi-channel is BN + ReLU + 1×1 Conv + BN + ReLU + 3×3 Conv. The initial layer is made up of a 7×7 conv and a 3×3 max pool. The convolution kernel has relatively small size and number. Therefore, the training parameters of the whole network will be relatively reduced. The transition layer of channel connection is composed of 1×1 convolution and 2×2 aggregate pooling. In the transition layer, the average pool sampling function is used to change the feature size and reduce the feature dimension, so as to reduce the model parameters. Finally, feature mapping inputs to the full connection layer through global pooling, which outputs the final fault diagnosis result.

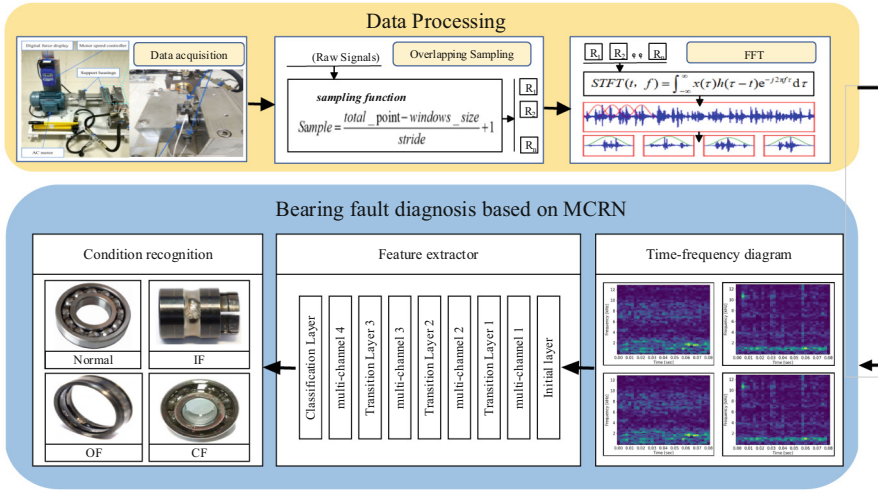


Fig. 3. Flow chart of bearing fault diagnosis using MCRN.

Table 1. Model parameters.

Layers	Output Size	Parameters	
Initial layer	17 × 9	7 × 7 conv 3 × 3 max pool	
Multi-channel Block (1)	17 × 9	1 × 1 conv 3 × 3 conv	× 4
Transition Layer (1)	8 × 4	1 × 1 conv 2 × 2 average pool	
Multi-channel Block (2)	8 × 4	1 × 1 conv 3 × 3 conv	× 4
Transition Layer (2)	4 × 2	1 × 1 conv 2 × 2 average pool	
Multi-channel Block (3)	4 × 2	1 × 1 conv 3 × 3 conv	× 4
Transition Layer (3)	2 × 1	1 × 1 conv 2 × 2 average pool	
Multi-channel Block (4)	2 × 1	1 × 1 conv 3 × 3 conv	× 4
Classification Layer	1 × 1	1 × 1 global average pool	

4 Experiment

4.1 Bearing Fault Detection of IMS Datasets

IMS Datasets is a full life cycle bearing experiment that provides rich data for bearing fault diagnosis. Figure 4 shows the IMS bearing test bench at the University of Cincinnati. The AC motor keeps a constant rotation speed of 2000 RPM and links to the shaft with friction bands. The shaft has four ZA-2115 double-row roller bearings. A spring mechanism applies 6,000 libraries of radial load to the bearings. All the bearings are force-lubricated. The sampling frequency of the sensor is set to 20 kHz. The IMS datasets contain three sub datasets, each of which records the whole process of bearing from normal operation to damage. This section uses the datasets of Bearing 1, Bearing 2, Bearing 3, and Bearing 4. The corresponding types are outer ring fault, normal, outer ring fault, and rolling element fault.

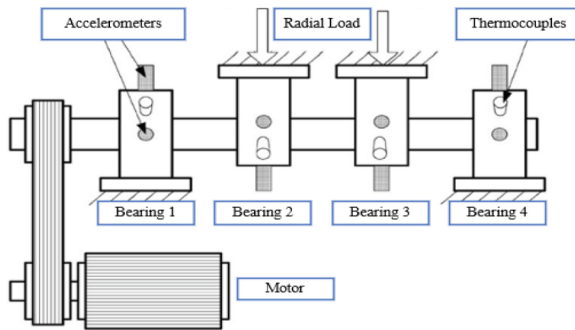


Fig. 4. IMS Bearing Test Bench.

The IMS experimental data set is shown in Fig. 5. For example, the states of Bearing-1 are relatively stable before 5410 min. But between 5410 and 5520 min, there is a small variation in the RMS, which suggests that the bearing has an early failure. Between 7020 and 9000 min, there is a fluctuation in the RMS, which suggests that the fault level is at the middle stage. The RMS increases after 9000 min, and reaches the maximum value at 9790 min, which means that the bearing has reached life limit. In the IMS Bearing datasets, bearing1 has no fault, and the vibration signal of 0110 min is taken as the normal data point. Bearing2 and Bearing3 have different degrees of outer ring failure in IMS experiment. Between 5410 and 5520 min, the vibration signal represents the early outer ring fault in Bearing 1. The early outer ring fault in Bearing3 is indicated by the vibration signal from 58900 to 59690 min. The vibration signal of 16501760min in Bearing4 is taken as the data point of early rolling body failure. There are 4,305 samples in each category.

The IMS experimental data set is shown in Table 2. In all 17,220 samples divided into a training set and a test set in a 7:3 ratio. In order to simulate the environmental noise of different degrees in actual engineering production, we add the Gaussian white noise of 0 dB, -1 dB, -2 dB, -3 dB and 4 dB into the vibration signal to build the test set respectively.